An Overview of Research Methods on Orthodontic Alloys and Ceramics

1

Spiros Zinelis and William A. Brantley

1.1 Introduction

Four clinically popular archwire alloys (stainless steel, cobalt-chromium-nickel, beta-titanium, and nickel-titanium) are currently used with brackets for tooth movement, and metallic brackets are manufactured from stainless steel and titanium [1]. Single-crystal (monocrystalline) or polycrystalline aluminum oxide (alumina) brackets are often used in place of metallic brackets because of much better appearance match to tooth structure, and there has also been interest in zirconium oxide (zirconia) for brackets [1].

For successful clinical performance, it is essential that these orthodontic alloys and ceramics have the appropriate properties to withstand clinical manipulation and the oral environment. Consequently, the necessary in vivo physical and mechanical properties must be defined, and these materials must be characterized appropriately for assurance that their properties are suitable for clinical conditions.

The first portion of this chapter will summarize some important current research areas for orthodontic materials: mechanical testing of the wire alloys and ceramic brackets, evaluation of the corrosion resistance of the wire alloys, use of x-ray diffraction to determine the structure of the wire alloys, and thermal analysis techniques to determine the structure of nickel-titanium archwires. Although not discussed in this chapter for the sake of brevity, thermal analysis can also be profitably employed to characterize the elastomeric impression materials and polyurethane modules used in orthodontics [1].

S. Zinelis (✉)
Department of Biomaterials, School of Dentistry, University of Athens,
Thivon 2 Goudi, Athens 11527, Greece
e-mail: szinelis@dent.uoa.gr

W.A. Brantley
Division of Restorative, Prosthetic and Primary Care Dentistry, College of Dentistry,
The Ohio State University, 3005L Postle Hall, 305 W. 12th Ave.
Columbus, OH 43210, USA

T. Eliades (ed.), *Research Methods in Orthodontics*,
DOI 10.1007/978-3-642-31377-6_1,

The second portion of this chapter will describe the preparation of orthodontic materials for microscopic examination and the important examination techniques. The materials are typically resin-embedded, then ground and polished, and sometimes chemically etched. The surfaces of these prepared materials, or other orthodontic materials in their bulk appliance form, are generally studied with the scanning electron microscope (SEM), which has largely replaced the optical microscope because of its vastly greater depth of focus and much wider range of magnifications available. Elemental compositions of orthodontic materials can be conveniently determined by energy-dispersive spectrometric analysis (EDS) with the SEM or by wavelength-dispersive spectrometric analysis with the electron microprobe. Recently, the technique of microtomography, which uses x-rays to create cross sections of objects at the microscopic level, has been employed to gain new insight into dental materials.

1.2 Mechanical Testing of Orthodontic Wires and Ceramic Brackets

The mechanical properties of orthodontic wires are best determined using the tension test and an electronically controlled universal mechanical testing machine with a straight archwire segment. An extensometer attached to the wire is employed to determine the change in a central gauge length (such as 1 in. or 10 mm), and the force developed within the wire during the tensile loading is sensed by a load cell. It is highly important that the load cell and extensometer be calibrated to obtain accurate results. Special wire grips must be employed, along with some strategy (such as surrounding the test specimen with metallographic abrasive paper) to prevent wire slippage within the grips. While not of clinical relevance, the wire segment can be loaded to failure, so that the ductility (percentage elongation) can be measured. Special breakaway extensometers are available for this purpose. Otherwise the extensometer should be removed from the test specimen after evident permanent deformation has occurred and the percentage elongation determined by fitting together the two halves of the fractured specimen.

Figure 1.1 shows tensile stress–strain curves for stainless steel, cobalt-chromium-nickel, Nitinol™ (3 M/Unitek), and Japanese NiTi [2] orthodontic wires, subsequently marketed as Sentinol™ or Sentalloy™ (Dentsply GAC International). The much lower elastic modulus of the nickel-titanium alloys is evident, along with the difference between elastic ranges of the nonsuperelastic Nitinol™ and superelastic Japanese NiTi. The latter has nonlinear elastic behavior, since stress and strain are not always linearly proportional below the elastic limit (end of upper superelastic plateau below point b) [2–4].

Determination of elastic modulus (E) and yield strength (YS) of a linearly elastic alloy from the tensile stress–strain plot is described in textbooks [3, 4], and reports of tensile properties of orthodontic wires are available [5, 6]. An important clinical property of an orthodontic wire is *springback*, which is defined as (YS/E) [7]. This relationship for springback is used to indicate the practical tensile elastic strain recovered

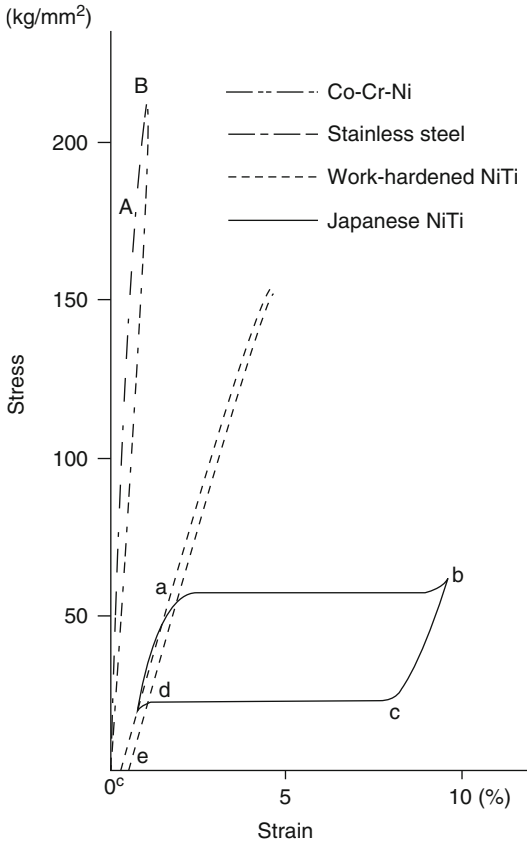

Fig. 1.1 Comparison of tensile stress–strain curves for 0.016 in. diameter stainless steel, Co-Cr-Ni, nonsuperelastic Nitinol™, and superelastic Japanese NiTi wires (From Ref. [2] and reproduced with permission from American Association of Orthodontists)

when the wire is unloaded, rather than (PL/E), where PL is the proportional limit, since orthodontists may activate wires into the permanent deformation range.

Mechanical properties of orthodontic wires are generally measured in the clinically relevant mode of bending, which is much more convenient to perform than the tension test. Figure 1.2 shows cantilever bending plots for stainless steel, Nitinol™, and Chinese NiTi (marketed as Ni-Ti™ by Sybron/Ormco) orthodontic wires, using 5 mm test spans appropriate for interbracket distances [8]. The effect of test span length on springback is pronounced, when comparing the original cantilever bending plots for Nitinol™ with 0.5 in. spans [9]. The Ni-Ti™ wire also exhibits superelastic behavior (and nonlinear elasticity), but the upper and lower superelastic plateaus evident with the tension test are not as sharply defined with the cantilever bending test [10], because of the variation in stress and strain over the wire cross section [1]. Springback in bending is much greater for superelastic NiTi wires than nonsuperelastic NiTi wires [10].

While the original version of American Dental Association Specification No. 32 had a cantilever bending test to evaluate mechanical properties of orthodontic wires [11], the current version [12] has three-point bending and tension tests. The specification

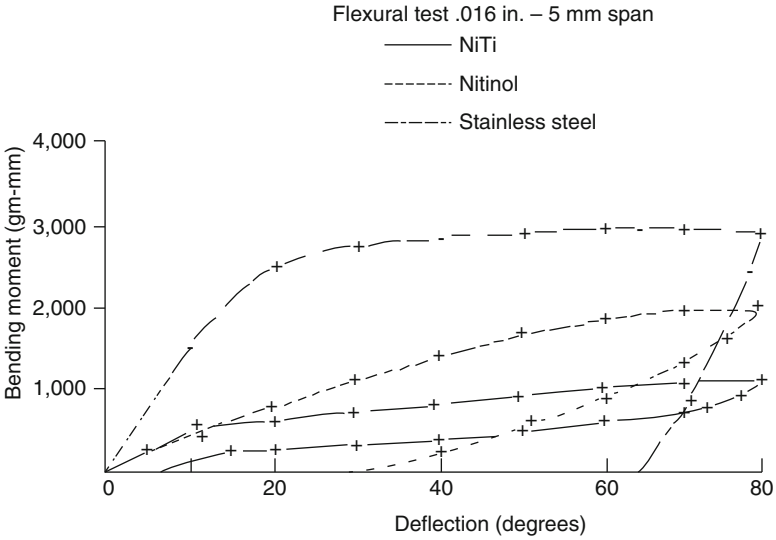

Fig. 1.2 Cantilever bending plots for 0.016 in. diameter stainless steel, Nitinol™, and Chinese NiTi orthodontic wires. For 5 mm test spans and bending deflection of 80°, springback is approximately 75° for Chinese NiTi and 50° for Nitinol™ (From Ref. [8] and reproduced with permission from American Association of Orthodontists)

testing mode depends on the manner in which the mechanical properties are given by the manufacturer. The wires are classified as type I or II, depending upon whether they exhibit linear or nonlinear elastic behavior, respectively, during unloading from temperatures up to 50°C. The bending test may be performed at room temperature (23 ± 2)°C for type I wires but must be performed at (36 ± 1)°C for type II wires. The test span between knife-edge supports is 10 mm, and the midspan deflection rate is 7.5 ± 2.5 mm/min. Type I wire specimens are bent to a permanent deflection of 0.1 mm, and the bending stiffness (units of N/mm) from the slope of the linear force–deflection plot and the bending force (N) for 0.1 mm permanent offset are determined. If the tension test is performed on a type I wire, the elastic modulus (GPa), 0.2 % offset yield strength (MPa), and percentage elongation are determined for a 20 ± 0.2 mm gauge length, using a crosshead speed between 0.5 and 2.0 mm/min. Type II wire specimens are tested only in three-point bending and are deflected to 3.1 mm. Forces during unloading are measured at deflections of 3.0, 2.0, 1.0, and 0.5 mm, along with the permanent deflection after unloading.

For ceramic brackets, it is essential to have sufficient strength to resist forces imposed during initial manipulation and bonding and the subsequent debonding. Such strength requires suitable resistance to fracture, since the ceramics used for brackets are brittle materials that fail by crack propagation, and ceramic brackets have historically shown a tendency for tie-wing fracture during debonding. The critical fundamental mechanical property is fracture toughness [13, 14], which is related to the force or energy for crack propagation. Fracture occurs with greater facility for single-crystal alumina brackets than polycrystalline alumina brackets where the irregular path of crack propagation is along grain boundaries [15].

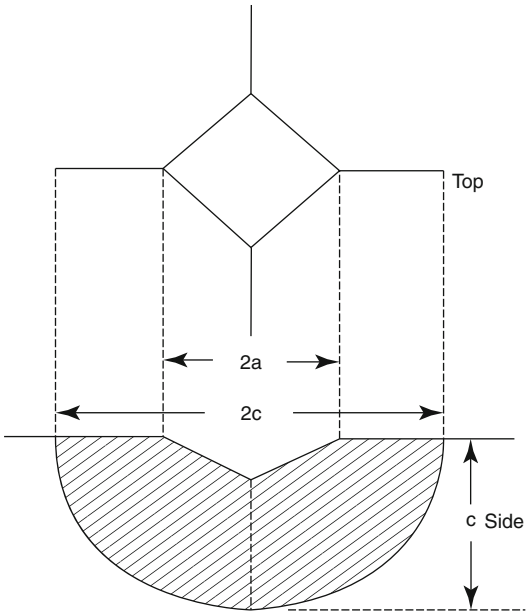

Fig. 1.3 Schematic illustration of Vickers hardness indentation and desired fracture pattern in ceramic material for determination of fracture toughness (From Ref. [21] and reproduced with permission from Academy of Dental Materials)

For convenience, the fracture toughness of dental ceramics is generally measured under plane-strain conditions as K_{Ic}, in which the tensile stress is applied perpendicular to the crack face in a crack-opening mode [4]. Several approaches have been used to measure the fracture toughness of bulk dental ceramics, including fractographic analysis, indentation methods, and bending tests with notched beams [16–21]. Figure 1.3 shows the idealized fracture pattern for the Vickers indentation technique, which is the only method that would permit measurement of fracture toughness for the very small ceramic brackets.

The Vickers indentation technique was used to obtain fracture toughness values of 3.60 and 5.22 MPa $m^{½}$ for two brands of polycrystalline alumina brackets [22]. However, these results were apparently obtained with radial cracks much shorter than the lengths of the diagonals for the indentations and thus may not be correct. Pham and colleagues [23, 24] found that the Vickers indentation technique did not yield appropriate long straight radial cracks emanating from the corners of Vickers indentations for five brands of polycrystalline alumina brackets, and the radial cracks followed the alumina grain boundaries in each ceramic. In contrast, Tilson and colleagues [25, 26] observed straight radial cracks in zirconia brackets (Hi-Brace™, Toray Ceram) with the Vickers indentation technique and obtained 3.92 ± 0.35 MPa $m^{½}$ for fracture toughness. However, SEM observations at high magnification revealed that the apparent straight radial cracks were the result of the very fine zirconia grain size, with crack propagation apparently still occurring along grain boundaries.

From these experimental results, it is recommended that future fracture toughness studies should focus on the bulk ceramic used to fabricate the brackets and that manufacturing efforts should be directed toward producing brackets of the highest

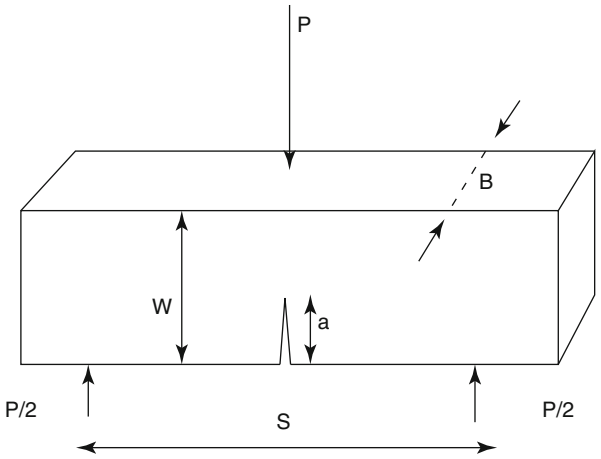

Fig. 1.4 Rectangular specimen geometry for single edge-notch technique used to measure fracture toughness. Appropriate specimen thickness or breadth (*B*) is necessary to have plane-strain conditions (From Ref. [28] and reproduced with permission from Quintessence Publishing Company)

purity ceramic with minimal surface cracks and porosity. Another approach for comparison of different ceramic brackets is to evaluate the force required to fracture the tie wings, which requires the use of a very small, well-controlled loading member [27]. A convenient technique for measuring the fracture toughness of bulk ceramic materials is the single edge-notch technique, schematically shown in Fig. 1.4 [28].

1.3 Corrosion Studies of Orthodontic Wire Alloys

Corrosion of orthodontic wires has become an active area of research, because of concern about biocompatibility. The major focus has been on nickel-titanium wires, which have potential to release nickel ions in vivo. A classic study, using potentiodynamic polarization [29], found that only the nickel-titanium alloy (Nitinol™) exhibited breakdown of passivity. X-ray analyses with the SEM suggested that loss of nickel could have occurred at the pitted regions. These results were consistent with clinical observations of stainless steel and Nitinol™ wires [30]. Long-term immersion of Nitinol™ was observed to have no effect on flexural properties and that occasional fracture was due to surface defects from manufacturing and not corrosion [31].

Figure 1.5 illustrates cyclic potentiodynamic polarization plots for three superelastic nickel-titanium wires, Nitinol SE™ (3 M/Unitek), Sentinol™, and Ni-Ti™ [1, 32, 33]. The directions of the forward and reverse scans are indicated by arrows. Similar results were found for nonsuperelastic Titanal™ (Lancer), Orthonol™ (RMO), and Nitinol™ wire alloys. The upper curve for each plot is the anodic region, and the lower curve is the cathodic region. These curves asymptotically approach each other at the zero-current potential [34]. The nickel-titanium wire alloys (and the other three orthodontic wire alloy types) have native surface oxide layers that provide corrosion resistance, and breakdown of the oxide layers (accom-

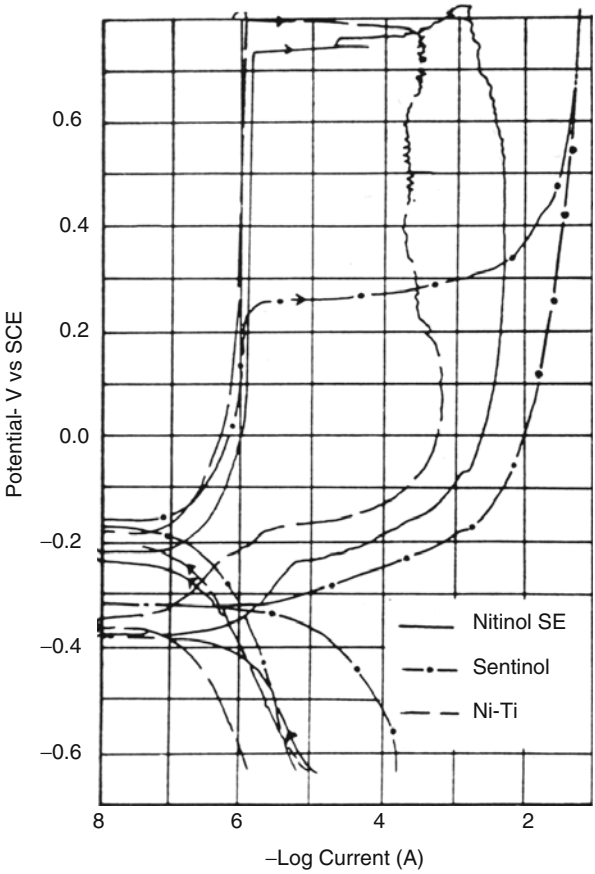

Fig. 1.5 Potentiodynamic polarization plots for three nickel-titanium orthodontic wire alloys [1, 32, 33] (From Ref. [1] and reproduced with permission from Georg Thieme Verlag (Stuttgart))

panied by pitting) can be seen in Fig. 1.5, where the current rapidly increases at sufficiently high anodic potentials. Because the wire surface has changed, the reverse scan does not follow the forward scan, and Fig. 1.5 shows that the zero-current potential has decreased for the reverse scan. The breakdown potential for the passive film depends on the surface roughness and oxide composition.

Corrosion studies have investigated breakdown potentials for oxide layers [35–37], ion release from wires [38–40], and galvanic coupling with brackets [41–44]. The in vitro corrosion of nickel-titanium wire products (including coated wires) has been compared [45–49] along with the potential of nickel-titanium wire for stress corrosion cracking [50]. An area of particularly active research interest has been effects of fluoride solutions (relevant to use of topical fluoride agents) on beta-titanium and nickel-titanium wires [51–59]. The beta-titanium wires, which are inherently the most biocompatible because of the absence of nickel, are susceptible to hydrogen absorption, leading to embrittlement and delayed fracture [51, 52]. The nickel-titanium wires also appear to be susceptible to hydrogen embrittlement [54]. The interested reader should consult the original articles for the diverse experimental procedures in these studies.

In closing this section, it is important to note that standardized in vitro corrosion tests may not adequately simulate the complex oral environment, where diverse chemical species and fluctuating stresses are present. This has been shown in studies of retrieved nickel-titanium archwires, where there was an apparent decrease in the grain size of the nickel-titanium wire [60] and an absence of significant nickel ion release in vivo [61]. Additional studies of this type are highly recommended for the future. Another very important related area for research is the cytotoxicity of the wire alloys. Studies generally show that the nickel-titanium alloys have low cytotoxicity [62] and that the surface quality of these alloys and the cobalt-chromium-nickel alloy Elgiloy [63] is an important factor.

1.4 X-Ray Diffraction

X-ray diffraction (XRD) is an important analytical tool in materials science for investigating the structure of metals. Orthodontic wires can be readily studied by conventional XRD, using a test specimen consisting of several adjacent segments of the wire and having a width greater than the incident x-ray beam size. Each crystalline phase has a characteristic XRD pattern, which is dependent upon crystal structure, lattice parameter(s), and atomic species in the unit cell. The principles and applications of XRD are discussed in a well-known textbook [64], and a succinct presentation of relevant information is also available [1] for people interested in orthodontic materials research.

For conventional XRD used to investigate orthodontic wire alloys, a beam of nearly monochromatic x-rays (typically Cu $K\alpha$) is used, and the XRD spectrum or pattern is recorded with a diffractometer. The relationship between the angle of incidence (θ) and wavelength for the x-ray beam and the lattice parameter(s) of the material being analyzed, in order to have a diffracted beam with x-ray waves in phase (yielding a strong peak), is given by Bragg's law. The diffraction angle recorded by the diffractometer is (2θ).

The crystal planes that yield the XRD peaks for a given material depend upon the structure factor. X-ray diffraction standards for powder specimens of materials, which have randomly oriented crystals, are maintained by the International Centre for Diffraction Data (ICDD). The standard for a material provides the relative intensities of the diffracting crystal planes and the corresponding interplanar spacings. These interplanar spacings are converted to the diffraction angles, using Bragg's law with the wavelength of the given characteristic x-rays from specific electron transitions in the source. When a material contains more than one phase, the XRD pattern contains the peaks from all of the phases.

X-ray diffraction analysis of several sizes of two stainless steel wire products showed that the 0.016 in. diameter and 0.017 in. × 0.025 in. wires of both products had a duplex austenite and martensite structure, rather than the completely austenitic structure [65]. It was found that heat treatment of one wire product converted this duplex structure to the austenitic structure, but the duplex structure persisted for the other product. The heat treatment responses were attributed to a difference in

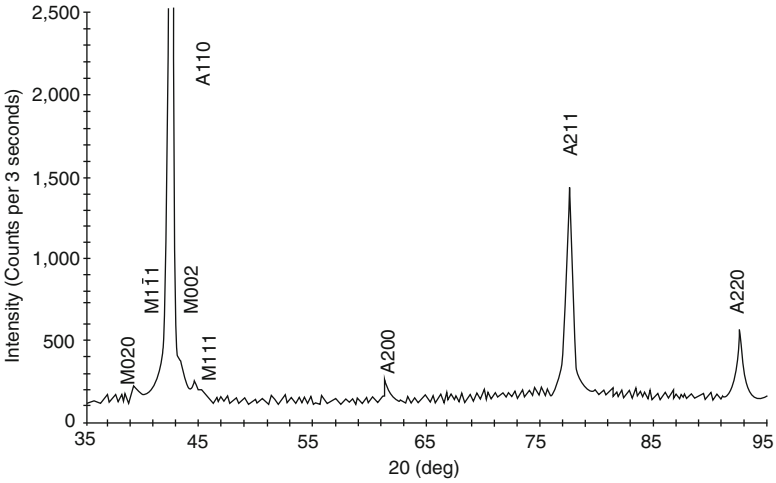

Fig. 1.6 X-ray diffraction pattern for 0.016 in.×0.022 in. Neo Sentalloy™ (From Ref. [1] and reproduced with permission from Georg Thieme Verlag)

carbon content for the wire products from the two manufacturers. The XRD pattern for as-received beta-titanium wire (TMA™, Ormco) had peaks for the body-centered cubic beta-titanium structure, which were broad with preferred crystallographic orientation, as expected for the work-hardened wire [1, 66].

Conventional x-ray diffraction has been used extensively to study nickel-titanium wires [1, 32, 66–68]. Figure 1.6 shows the XRD pattern for Neo Sentalloy™ (GAC) [66], in which the crystal planes in the austenite and martensite structures have been indicated. Although this wire alloy has shape memory in the oral environment, when it is in the fully austenitic condition, the XRD pattern in Fig. 1.6 also shows peaks for martensite because the analysis was performed at room temperature, which is below the austenite finish (A_f) temperature for Neo Sentalloy™, as shown in the next section. The much weaker intensity of the USE 220 austenite peak, compared to the 211 peak, referring to the relatively intensities in the ICDD powder standard [1], is indicative of preferred orientation.

Figure 1.7 shows the XRD pattern for Ni-Ti™ (Ormco) after heat treatment for 2 h at 600°C [1, 32], which causes complete loss of the superelastic behavior for this wire alloy [10]. The wire has the completely austenitic structure, indicating that the martensite start temperature (M_s) is below room temperature after the heat treatment, so that minimal austenite transformed to martensite when the wire was cooled to room temperature for the XRD analysis [1, 32]. The sharp XRD peaks are indicative of substantial stress relief after heat treatment and perhaps recrystallization of the wire structure with new, stress-free grains. There is also strong preferred orientation. Referring to the ICDD standard, the peaks in Fig. 1.7 correspond to the 110, 200, 211, 220, and 310 reflections.

An exciting recent development is the use of micro-x-ray diffraction (micro-XRD) to investigate orthodontic wires [69–73]. With the micro-XRD technique,

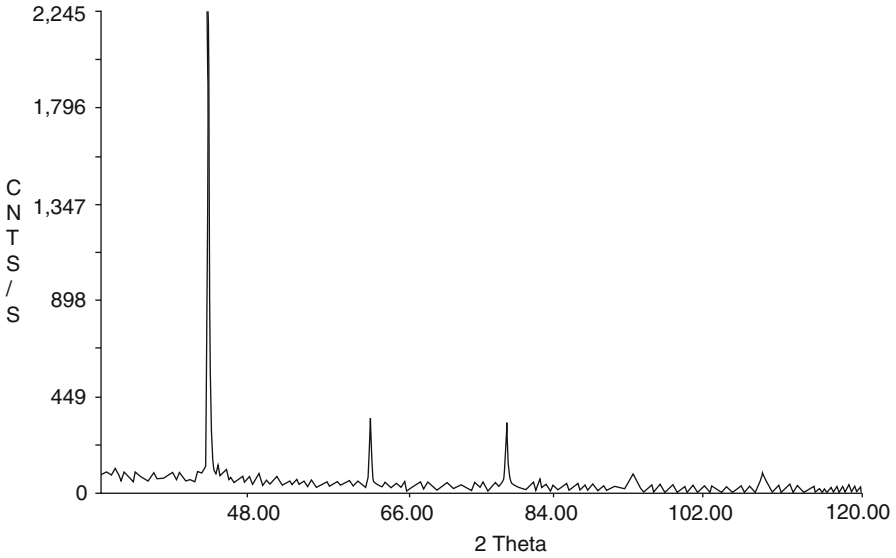

Fig. 1.7 X-ray diffraction pattern for 0.016 in. diameter Ni-Ti™, following heat treatment for 2 h at 600°C [1, 32] (From Ref. [1] and reproduced with permission from Georg Thieme Verlag)

which employs a relatively large tube current, the spot size for the incident x-ray beam can be as small as 100 μm. For example, analyses of tension and compression regions on bent wires, and of soldered and welded joints for orthodontic wires, become possible.

1.5 Differential Scanning Calorimetry (DSC) and Temperature-Modulated DSC

Conventional differential scanning calorimetry (DSC) has become the major analytical tool for study of the transformations of the NiTi microstructural phases with changes in temperature for the nickel-titanium orthodontic wires. Two classic articles [74, 75] describe the first reported use of DSC to investigate these wires, and there were several subsequent studies [76–78]. The current ANSI/ADA specification and ISO standard for orthodontic wires [12] stipulates the use of DSC to determine the A_f temperature for nickel-titanium wires. The advantages of DSC over XRD are its ability to determine the NiTi phases present at a given temperature, to investigate the phase transformation processes with changes in temperature, and to measure the enthalpy changes (ΔH) for these processes. The enthalpy changes provide insight into the transformation processes, which is not possible with x-ray diffraction or with the measurement of electrical resistivity changes. While the latter measurements can be readily performed over a range of temperatures, this is not generally possible with XRD apparatus.

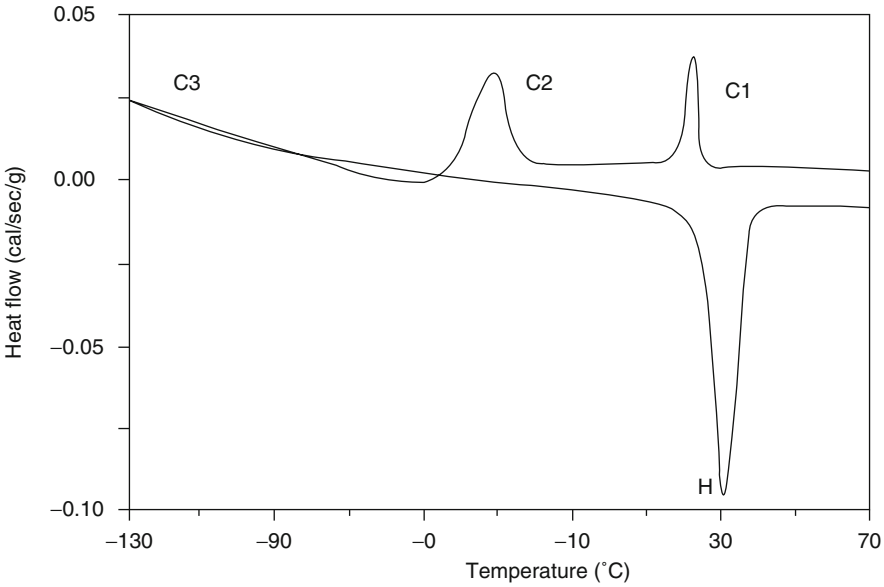

Fig. 1.8 Conventional DSC plot (thermogram) for Neo Sentalloy™ (From Ref. [76] and reproduced with permission from American Association of Orthodontists)

With conventional DSC, a small test sample of the experimental material (a few wire segments) is placed in one pan and an empty pan (typically aluminum) serves as the inert reference material [1]. Some investigators prefer to use indium as the reference material. Both pans are heated or cooled at a constant rate (typically 10°C/min), and the difference in heat flow (in units of cal/s/g or W/g) to the two pans to maintain the same temperature change for both pans is recorded as a function of temperature.

The conventional DSC plot for the shape memory wire Neo Sentalloy™ is shown in Fig. 1.8 [76]. The single peak (H) on the lower curve for the heating cycle suggests the direct transformation from martensite to austenite. The A_f temperature, at which the transformation to austenite has finished, is approximately 36°C. The upper curve for the cooling cycle has two peaks (C1 and C2), which correspond to transformations from austenite to R-phase and R-phase to martensite, respectively. (C3 was placed where low-temperature martensite peaks were previously found from measurements of electrical resistivity changes [79,80]).

Conventional DSC [76] shows that in vivo shape memory NiTi wire products have A_f temperatures lower than body temperature (37°C), whereas superelastic wire products have A_f temperatures that exceed body temperature (approximately 60°C for Nitinol SE™ and 40°C for Ni-Ti™). The nonsuperelastic Nitinol™ has A_f temperature of approximately 55°C and weak peaks (low ΔH values) [75, 76] corresponding to substantial quantities of stable work-hardened martensite in this wire.

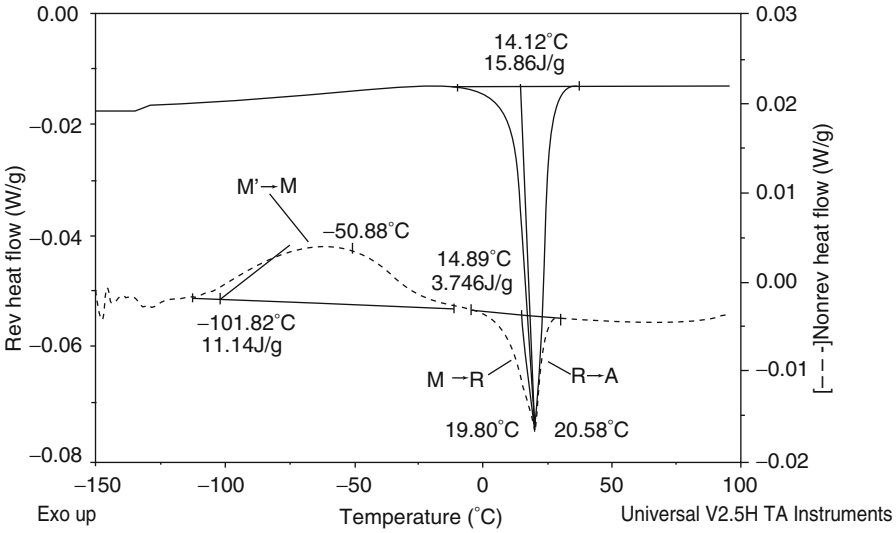

Fig. 1.9 TMDSC plots of reversing and nonreversing heat flow for heating cycle of Neo Sentalloy™, with phase transformation processes for peaks labeled (From Ref. [83] and reproduced with permission from American Association of Orthodontists)

The recently introduced technique of temperature-modulated differential scanning calorimetry (TMDSC) [81, 82] provides insight into phase transformation processes that is not possible with conventional DSC. (The generic term is TMDSC; use of the term *modulated differential scanning calorimetry* is specific to apparatus from TA Instruments.) With TMDSC, the linear heating or cooling rate is much slower (such as 2°C/min) to maintain a uniform temperature in the bulk specimen, and a small sinusoidal thermal oscillation (such as an amplitude of 0.318°C/min with a period of 60 s) is superimposed on the linear ramp. When selecting the thermal oscillation conditions, it is highly important to maintain a heating-only condition during the heating cycle and a cooling-only condition during the cooling cycle. Thin test specimens are needed, and helium is the preferred purge gas because of its high thermal conductivity, rather than nitrogen which is typically used with conventional DSC. Utilization of the small sinusoidal oscillation superimposed on the linear heating or cooling ramp allows mathematical subdivision of the total heat flow measured by conventional DSC into its reversing and nonreversing components with respect to temperature changes.

The advantages of TMDSC are evident in Fig. 1.9, which shows the heating cycle for Neo Sentalloy™ [83], compared to the heating cycle on the conventional DSC plot in Fig. 1.8. The dashed nonreversing heat flow curve in Fig. 1.9 shows that a two-step transformation from martensite to austenite occurs, which involves the intermediate R-phase. There is also a strong exothermic peak on the nonreversing heat flow curve arising from low-temperature transformation within martensite (designated as M′ → M for heating).

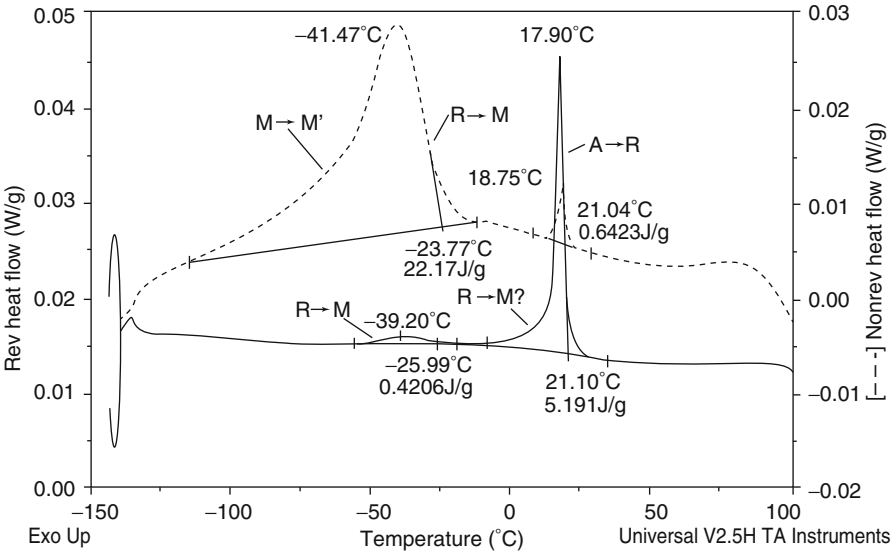

Fig. 1.10 Corresponding TMDSC plots of reversing and nonreversing heat flow for cooling cycle of Neo Sentalloy™ (From Ref. [83] and reproduced with permission from American Association of Orthodontists)

The corresponding TMDSC plots for the cooling cycle of Neo Sentalloy™ are shown in Fig. 1.10 [83]. The reversing heat flow curve has a large exothermic peak for the transformation from austenite to R-phase, which can be seen to have a small amount of nonreversing character. Possible transformations from R-phase to martensite are labeled on both the reversing and nonreversing heat flow curves. There is a large exothermic peak on the nonreversing heat flow curve (designated as M → M′ for cooling), which again corresponds to transformation within the martensite structure. As noted previously, low-temperature martensite transformations in NiTi orthodontic wires were originally reported from measurements of electrical resistivity changes [79]. Recent low-temperature transmission electron microscopy examination of 35°C Copper Ni-Ti™ wire has shown that twinning within martensite is the origin of this peak on the TMDSC nonreversing heat flow curves [84]. During both the heating and cooling cycles, the martensite structure undergoes twinning to relieve internal stresses in the microstructure. This low-temperature peak has been observed in all orthodontic wires examined by TMDSC in two studies [83, 85].

1.6 Metallographic Preparation

1.6.1 Background

Metallographic preparation is extensively used in order to reveal the true bulk structure of solid materials. The distribution of pores, presence of cracks or other internal

defects, quality of joints, and grain size and shape are only a few of the features that can be qualitatively and quantitatively determined by the analytical techniques (i.e., optical and electron microscopy). Sectioning, mounting, grinding, polishing, and etching are the main steps of metallographic preparation although the latter is applied only when the grain structure and microstructural phases are the subject of research. As a standard operating procedure, metallographic preparation must be characterized by reproducibility and reliability. Reproducibility is associated with the ability of a method to provide the same results for the same material, every time it is carried out, while reliability represents the ability of the method to provide the true structure of the material free of possible structural alterations (e.g., deformation and smearing) and other artifacts.

1.6.2 Sectioning

The main goal of sectioning is the removal of a conventionally sized, representative specimen from a larger sample. Although sectioning is routinely used in metallographic preparation of specimens from various applications, this is not the case in orthodontics where the specimens are of very small dimensions. Orthodontic wires can be easily cut by pliers, avoiding the use of sophisticated sectioning machines. Complete details on sectioning are not included in this chapter, but the reader can find extensive information elsewhere [86].

1.6.3 Mounting

In general, mounting is considered optional, and it may not be necessary for some bulk specimens. However, a small or oddly shaped specimen (e.g., an orthodontic bracket) should be mounted in order to facilitate handling during metallographic preparation Fig. 1.11. Standard molds usually have diameters of 25, 32, or 38 mm. Caution should be exercised about the final thickness of mounted specimens, as very thin mounted specimens are difficult to handle, and the flatness of very thick ones is difficult to preserve during metallographic preparation.

The first criterion for the selection of the proper mounting material and technique is the protection and preservation of the sample. Delicate and fragile samples may be subjected to physical damage or microstructural alterations due to the heat and pressure required by some mounting materials. Ideally the mounting material should have similar grinding and polishing characteristics as those of the sample. Additionally, the mounting material should effectively resist physical distortion caused by the heat developed during grinding and polishing and withstand exposure to suspensions, lubricants, and etching solutions. The mounting material should have low viscosity so that it can easily penetrate crevices, pores, or other irregularities in the sample. In addition, the mounting material should be easily manipulated and stored and should present no health hazards to the operator. It should not be susceptible to the formation of any defects (e.g., cracks and pores) and should be

Fig. 1.11 Three pieces of orthodontic wire embedded in acrylic resin (*yellow cylinder*) reinforced by mineral fillers to provide good ability for achieving planar surface and good edge retention. Cylinder diameter is 25 mm

available for purchase at a reasonable cost. Sometimes an electrically conductive mount is desirable, such as for electrolytic polishing and scanning electron microscopy analysis. Currently, there is no mounting material that fulfills all of the aforementioned requirements, and a variety of materials and methods are available. Proper selection is considered the one that meets the most critical requirements for each combination of material and subsequent analytical technique.

The available mounting materials can be classified into two groups: (1) materials that require the application of heat and pressure and (2) materials that can be poured into a room temperature mold [86]. The technique used with the first group of materials is termed *hot mounting*, and the technique used with the second group is termed *cold mounting*. In the hot mounting technique, the specimen is placed in the mounting press, and after the pouring of resin, the mounted specimen is processed under high pressure and heat. The mounting materials used for this technique are (a) thermosetting resins which cure at elevated temperatures and (b) thermoplastic resins which soften or melt at high temperatures and harden during cooling to room temperature. Epoxy, acrylic, and polyester materials are used in cold mounting. Epoxies are characterized by low shrinkage and excellent adhesion to most materials but have relatively long curing times. Acrylics and polyesters are catalyzed systems and have short curing times.

1.6.4 Grinding and Polishing

The next steps of metallographic preparation after mounting are the grinding and polishing of the sample surface. The purpose of grinding is primarily to remove damaged or deformed material at the sample surface and to produce a plane surface that will be easily removed during the polishing step. Successive steps with finer abrasive particles are employed during this step to remove material from the sample surface until the required result is reached. Grinding and polishing are commonly

carried out in special designed metallographic machines in which the abrasive papers are placed on a rotating wheel and the sample surface is firmly placed sequentially against each abrasive paper. Significant heating of the surface during the initial coarse grinding step is avoided by using a copious amount of water or another liquid as a coolant. The aim of polishing is to remove the surface damage introduced during grinding, which is accomplished with several steps of successively finer abrasive particles.

During polishing, the abrasive particles are suspended in a liquid and retained among the fibers of special metallographic cloths. Diamond and aluminum oxide suspensions (slurries) are most commonly used for polishing. Generally, the final abrasive particle size is 0.5 μm, which is approximately half the wavelength of visible light, so that the polishing scratches on the sample surface cannot be seen visually or in the optical microscope. While the principles for grinding and polishing are straightforward, the reader should be aware that both procedures are much more complicated and that revealing the true microstructure is always a challenge for the metallographer. Selection of the appropriate metallographic technique and achieving an artifact-free sample surface are the two milestones of proper sample preparation. Decades of experience have led to grinding and polishing procedures that are appropriate for each material type [87]. For example, the preparation procedure for a bracket-adhesive resin-tooth interface requires a completely different procedure compared to that for an orthodontic Ni-Ti alloy, which is considerably different from the grinding and polishing procedure for a Co-Cr archwire. All these procedures have been summarized in an excellent reference book [87].

1.6.5 Etching

Although some microstructural features (e.g., pores, cracks, pits, and nonmetallic inclusions) may be observed in the as-polished condition, the microstructure is usually revealed only after etching. A well-polished sample surface will not reveal its microstructure because light is uniformly reflected, and the eye cannot distinguish small differences. Generally, only features that show greater differences than 10 % in reflectivity can be viewed without etching, such as features with large differences in hardness that cause surface relief formation or with strong color differences. In the vast majority of cases, image contrast must be produced.

Although metallographic contrasting methods include physical, optical, and electrochemical etching techniques, chemical etching is most extensively used to reveal the microstructures of samples. Alternative etching techniques have been developed for cases in which an effective etching solution cannot be found such as for chemically stable ceramics (e.g., ZrO_2 and Al_2O_3). Etching solutions are provided by the relevant literature in a form similar to cooking recipes. The metallographer has to produce the proper etching solution according to the material and the microstructural feature under study. The results of chemical etching are very sensitive to temperature, composition, and pH alterations of the etchant employed, and thus considerable care should be taken to follow the given instructions. Figure 1.12

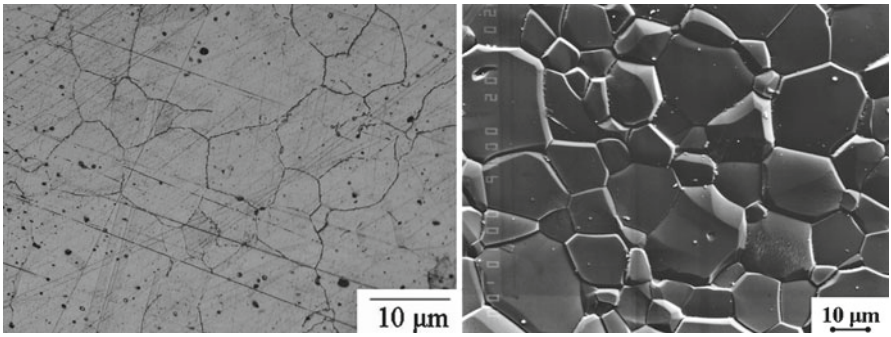

Fig. 1.12 *Left*: Microstructure of austenitic stainless steel alloy revealed after etching with solution composed of 1 g picric acid, 5 mL HCl, and 100 mL ethanol. *Straight lines* are scratches created during grinding and polishing steps (original magnification 200×). Photomicrograph was obtained with optical microscope. *Right*: Microstructure of alumina ceramic bracket after thermal etching. Backscattered electron image was obtained with scanning electron microscope (original magnification 100×)

(left) shows the microstructure of an austenitic stainless steel alloy used for the production of orthodontic brackets by the metal injection-molded (MIM) technique [88] and (right) the grain structure of a ceramic bracket.

It can be seen that metallographic preparation is a multistage procedure with a variety of materials and techniques potentially involved, and the metallographer should be extremely cautious in order to avoid artifacts and/or contamination during the preparation procedures that might significantly alter the true microstructure of the sample.

1.6.6 Light (Optical) Microscopy

Despite the evolution of advanced electron-optical metallographic methods, such as use of the scanning electron microscope (SEM) and transmission electron microscope (TEM), the optical microscope remains an important and easy technique for the study of microstructures. Polished or etched samples can be directly viewed in the optical microscope, whereas imaging with the SEM and TEM requires further preparation steps and advanced facilities. Specimen preparation can be particularly time-consuming for TEM, in which the extremely thin foil specimen must be transparent to the primary electron beam. (This advanced materials science technique will not be discussed in this chapter.) All examinations of microstructure should be done from the lowest (nominal magnification 50×) to highest magnifications (1,000×) to characterize the microstructural features. However, if some microstructural features are too fine to be identified with the optical microscope, other techniques that provide higher magnifications must be employed.

Both as-polished and etched surfaces can be easily investigated, although some features are more readily identified in the former condition because they are not

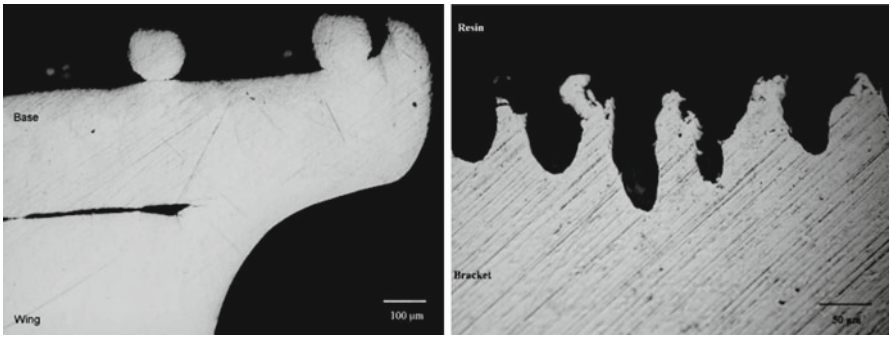

Fig. 1.13 Cross-sectional images obtained by bright-field optical microscopy. Large gaps are prominent along base-wing interface in *left image* (original magnification 100×). *Right image* shows cross section of single-piece bracket with laser-structured adhesive base (original magnification 200×)

obscured by etching detail. Optical microscopy has been extensively used to determine the microstructures of several metallic orthodontic brackets (Fig. 1.13) [88–90]. In addition to the use of conventional bright-field illumination, image contrast can be enhanced by oblique lighting, dark-field illumination, phase contrast, interference contrast, and examination under polarizing light. Image analysis software is available that can provide quantitative information about microstructural features such as percentage of porosity, shape and size of constituents, and interparticle distance, and such software can also be utilized for images obtained by other methods such as SEM and EPMA (electron probe microanalysis).

However, in some cases (e.g., broken parts such as debonded brackets from dental enamel) observation and photography at very low magnification should be performed. This macrophotography procedure can be performed using typical cameras, perhaps aided by use of a macrolens or close-up lens attachments. In the research laboratory, the use of a stereomicroscope equipped with cameras for photography is more common. Nominally, macrophotography uses magnifications from less than 1× to 50×. Correct lighting is critical to properly emphasize details on the sample being photographed and to provide adequate contrast and even illumination without reflection or glare. In orthodontics macrophotography is commonly used to investigate mesh-type brackets and characterize the fracture mode through the estimation of percentage retained resin after bracket debonding from enamel (Fig. 1.14).

1.6.7 Scanning Electron Microscopy (SEM)

The scanning electron microscope is probably the most widely used analytical technique in materials science worldwide. Useful magnifications start from very low (6×) and extend to 150,000×, thus closing the gap between optical microscopy and transmission electron microscopy. Additionally, compared to the optical microscope, the SEM provides higher resolution and depth of focus by one and two orders

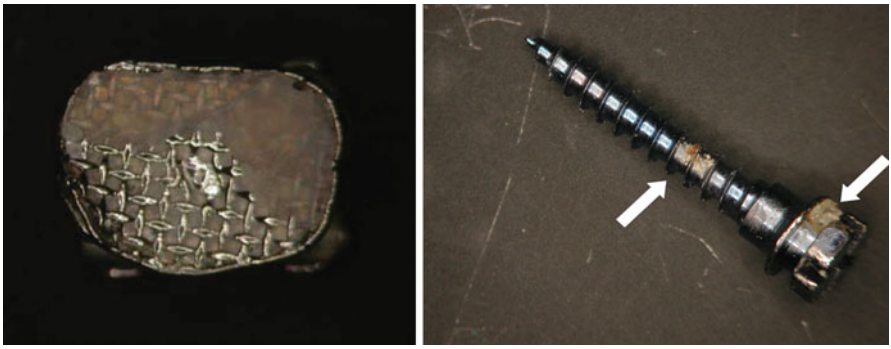

Fig. 1.14 Stereomicroscopic images of orthodontic appliances. *Left*: Surface of bracket debonded from enamel after shear bond strength test. Presence of retained resin is readily distinguished from bracket surface. *Right*: Retrieved orthodontic miniscrew implant showing intraoral aging-induced integuments (indicated by *arrows*)

of magnitude, respectively. Moreover, the SEM yields clear images of rough surfaces, polished surfaces, and etched surfaces, although focusing can be more difficult with very smooth surfaces. Elemental analysis with the SEM is carried out with the use of detectors that determine the energy or wavelength of the characteristic x-rays (created by the incident primary electron beam) that are emitted from each element in the sample. Good lateral resolution can be achieved. Given that the SEM images are built by the raster scanning of successive primary electron beams across the sample surface, individual line scans can be acquired that portray the distribution of elements of interest in the sample. While the conventional SEM is extensively used in a wide range of applications in materials research, recent advancements can provide imaging of nonconductive specimens (low-vacuum SEM) and wet samples at 99 % relative humidity (environmental SEM), dramatically expanding the capabilities of this method.

The SEM uses an electron beam emitted from a heated tungsten cathode filament and focused to a small diameter (approximately 5–15 nm) by a system of magnetic lenses. Accelerating voltages vary from 0.1 kV to maximum generally of 30 kV, while the beam current ranges from 10^{-7} to 10^{-8} A. The whole system is placed under high vacuum, and the incident primary electron beam raster-scans the specimen surface as in a cathode ray tube used for image formation on a television screen. The interaction between the primary electron beam and the specimen yields secondary and backscattered electrons along with other radiation that can be collected by the detectors to form images and provide analyses of elements in the overall sample or in the individual microstructural phases or constituents.

Secondary electron images (SEI) are formed by the secondary electrons emitted from the specimen surface. These electrons are created by interaction of the incident beam with loosely bound electrons in the elements comprising the sample. They are emitted from the uppermost layers of the material with an excitation depth up to 10 nm below the specimen surface, and thus they provide a very clear image of surface morphology. This property, along with the increased depth of focus of the

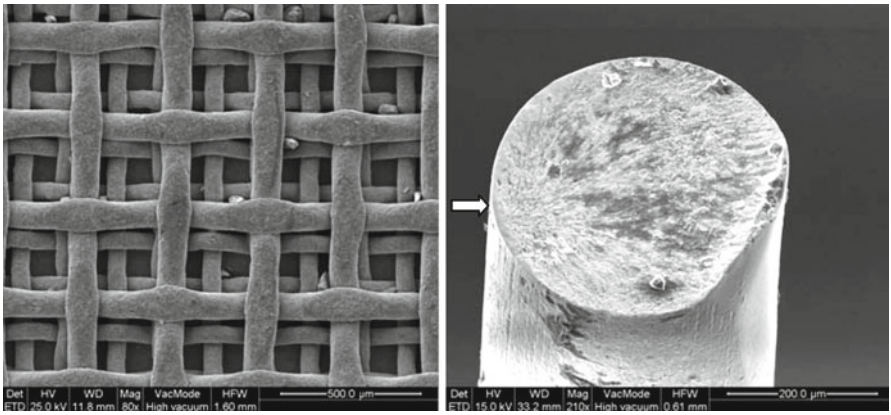

Fig. 1.15 *Left*: Multilevel foil mesh of contemporary metallic bracket. *Right*: Fracture surface of niti archwire that failed during clinical use. Fracture pattern is characterized by fibrous texture, and origin of fracture is indicated by *arrow*. Shear lip at right edge of wire was final region to undergo fracture

electron beam, can provide very clear images for specimens with multilevel surfaces. Examination of mesh patterns from different brands of orthodontic brackets and analysis of the fracture surfaces of orthodontic wires have been carried out using this type of imaging [88–91] (Fig. 1.15).

Backscattered electron images (BEI) provide atomic number (Z) contrast for the material, because the energy distribution of backscattered electrons created by the incident electron beam depends primarily on the atomic number of the material. Thus, regions composed of different elements, or more precisely regions with difference in mean atomic number, can be readily discriminated by this mode of SEM operation. Such contrast is useful for microstructural phase discrimination, and thus BEI are extensively used for the investigation of multiphase materials such as soldering alloys for stainless steel orthodontic brackets (Fig. 1.16) [92]. This type of imaging is especially suitable for quantitative evaluation of microstructural geometry that employs image analysis procedures.

Two more modes of SEM operation known as cathodoluminescence and thermal wave imaging have limited applications to orthodontic research, and they are not included in this section.

1.6.8 Electron Probe Microanalysis (EPMA)

In electron probe microanalysis (EPMA) also utilizes a primary electron beam of high intensity is accelerated at generally 5–30 kV and focused on a small area. The specimen microvolumes, which are again excited by scanning the beam over the target, produce two types of spectra [93]. The first type, commonly known as bremsstrahlung ("braking radiation") and having a continuous spectrum, originates from the range of interactions between the electrons and atoms of the material

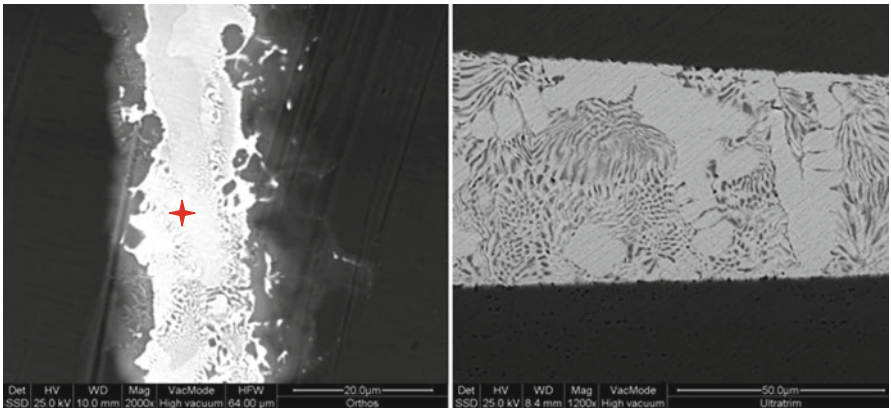

Fig. 1.16 Backscattered electron images from polished surfaces of soldered brackets. brazing zones are clearly distinguished from base (*left region*) and wing (*right region*) bracket components. *Red cross* identifies point for spot analysis described in next section on EPMA. The *left image* shows transition zone between brazing alloy and two brackets components (original magnification 2,000×). In contrast, *right image* shows prominent two-phase eutectic structure regions in brazing alloy and no transition zone between base and wing components of bracket (original magnification 1,200×)

through which they are passing. The second is a characteristic radiation for the particular element with a distinct line spectrum in each case. The inner shell electrons of the target atoms are primarily ionized by the incident electron beam and, upon relaxation to the ground state, emit characteristic x-rays that correspond to the energy loss for the particular transition in the excited element. Since these characteristic x-rays are independent of the chemical environment of the atoms, they are suitable for elemental analysis. When this emission occurs, these characteristic x-rays can be acquired by suitable detectors and analyzed qualitatively and quantitatively by WDS (wavelength-dispersive spectroscopy) or EDS (energy-dispersive spectroscopy) [93].

EPMA offers three analysis modes, which will be described in the following paragraphs.

1. Spot (point) analysis involves the acquisition of a spectrum at a selected point. This type of analysis is very convenient for the elemental analysis of specific regions, such as small regions of phases, foreign particles, and inclusions. Figure 1.17 illustrates a typical spectrum showing the quantitative results for the soldering alloy of Fig. 1.16.
2. Area scan analysis involves the presentation of the elemental distributions in the form of maps. This type of analysis is employed to identify the overall surface distribution of each element. Figure 1.18 shows the BEI of a soldered orthodontic bracket made from a stainless steel alloy in this presentation format. The base and wing components were soldered using a soldering alloy with higher mean atomic number. Elemental mapping reveals that Au is solely found in the soldering alloy, while Ni has maximum values at the transition zone with the base and wing components. In addition, some Fe diffusion is evident at the transition zone.

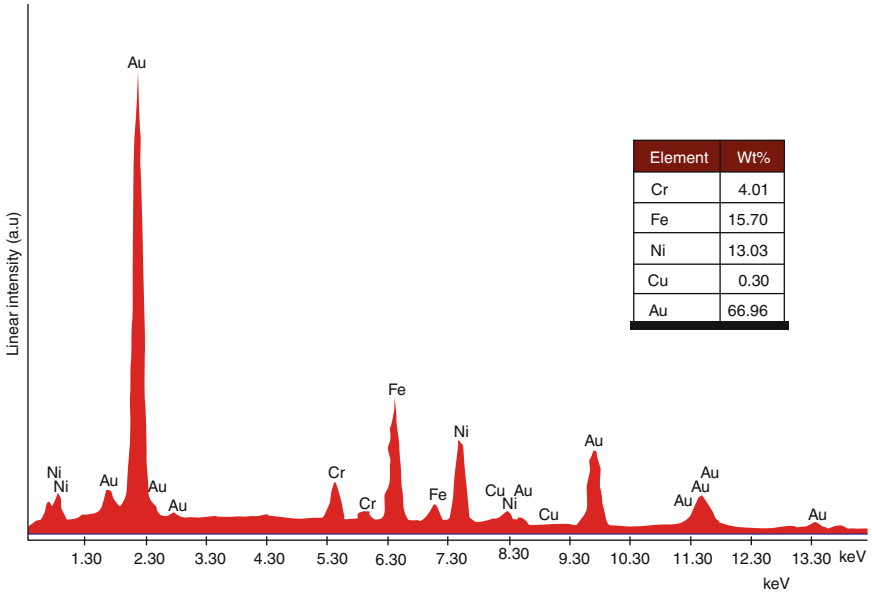

Fig. 1.17 Spectrum showing energy-dispersive x-ray microanalysis analysis of brazing filler material, acquired from *red spot* in Fig. 1.16. Table summarizes quantitative results of elemental weight percentages

3. Line scan analysis where the elemental gradients along a linear direction are measured. This analysis is very helpful to understand the variation in concentration of each element, information which is not so clear in area mapping. Figure 1.19 presents the concentration profiles of Au, Fe, Ni, and Cr for this example of a brazed orthodontic bracket.

Energy-dispersive spectrometric (EDS) analyses have been extensively used to analyze the elemental composition of orthodontic alloys [43, 44, 88, 89, 92], ionic release comparing the elemental compositions before and after intraoral aging [61, 90] of metallic orthodontic materials, and the distribution of intraoral integuments [60, 94].

1.6.9 Quantitative Image Analysis

The introduction of digital imaging and image processing has given a tremendous boost in the quantitative evaluation of microstructural features of materials. Generally, an image acquired with good resolution and contrast can be further enhanced by image analysis software for the quantitative evaluation of various features of interest (e.g., distance between specific points, interparticle distance, shape of phases or grains, percentage of porosity, percentage of area covered for the evaluation of fracture mode). In orthodontics, image analysis processing has also been used to characterize the fracture mode of brackets and the cohesive/adhesive nature of the interfacial failure process for different adhesive systems (Fig. 1.20).

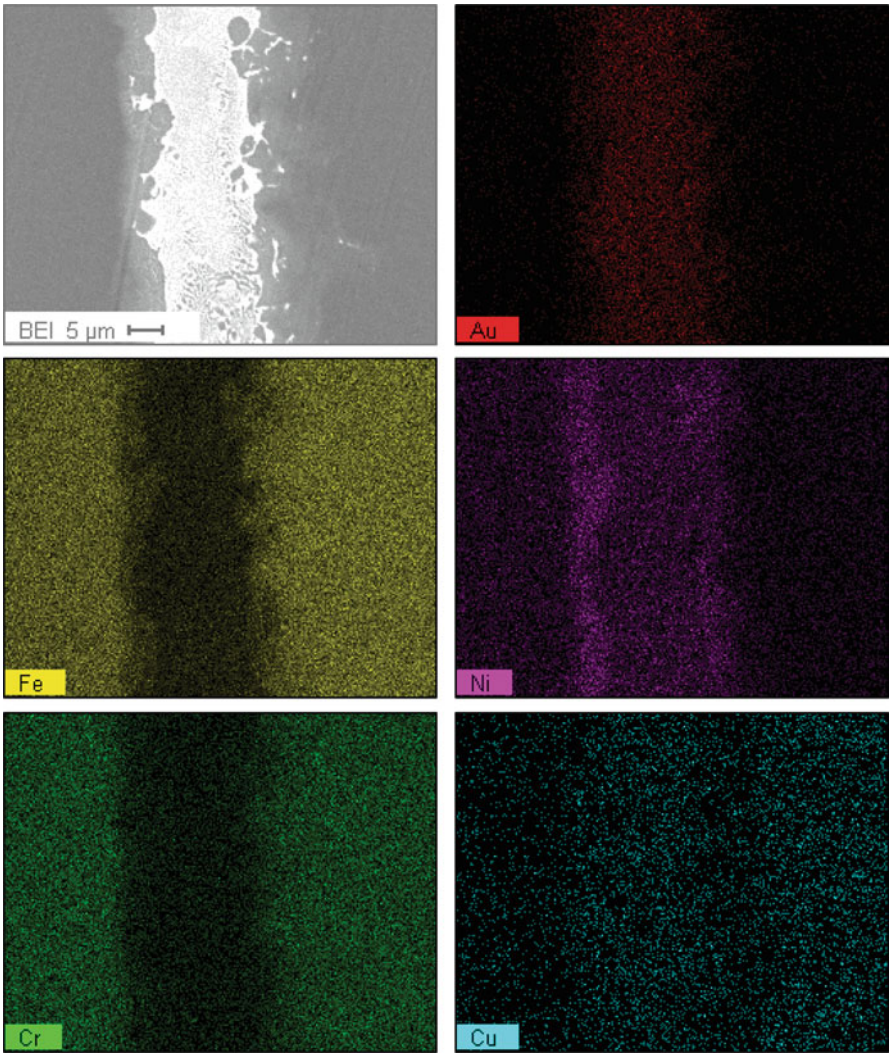

Fig. 1.18 Backscattered electron images for cross section of bracket consisting of two components (base and wing) joined together with brazing alloy. Maps show elemental distributions for Au, Fe, Ni, Cr, and Cu

1.6.10 Microcomputerized X-Ray Tomography (Micro-CT)

Computer tomography and image processing are extensively used in the medical field for the development of virtual models. In the last decade, new benchtop models for materials characterization were developed and are currently commercially available. These micro x-ray scanners employ the same principle as for medical tomography but with an isotropic resolution up to some hundreds of nanometers. A

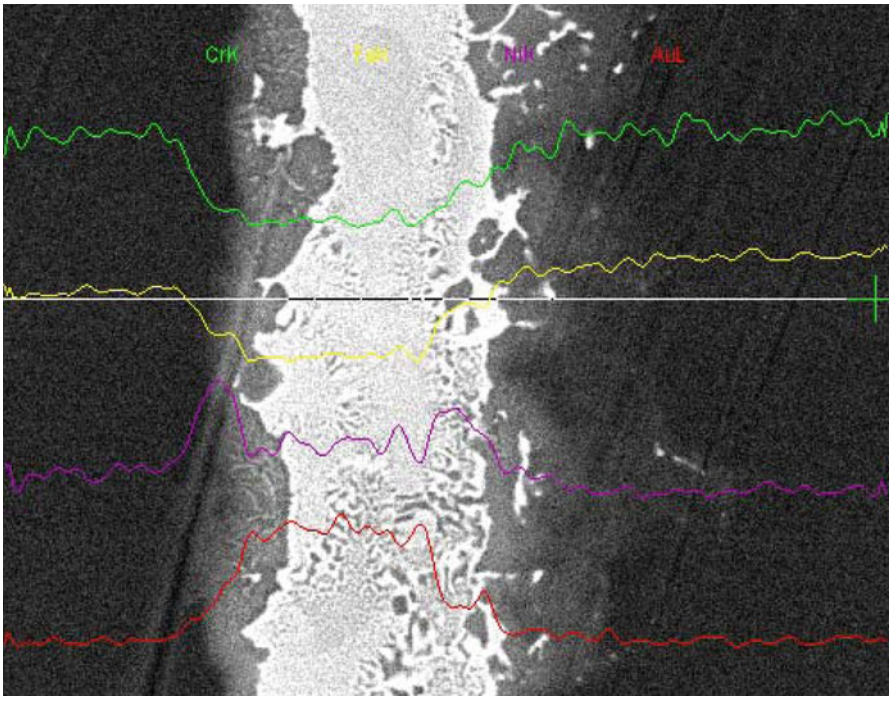

Fig. 1.19 Line scans demonstrating variation of four elements from base (*right*) to tie-wing (*slot*) area (*left*). *White horizontal line* shows specific location of linear region in which elemental concentration profiles of Cr, Fe, Ni, and Fe were determined

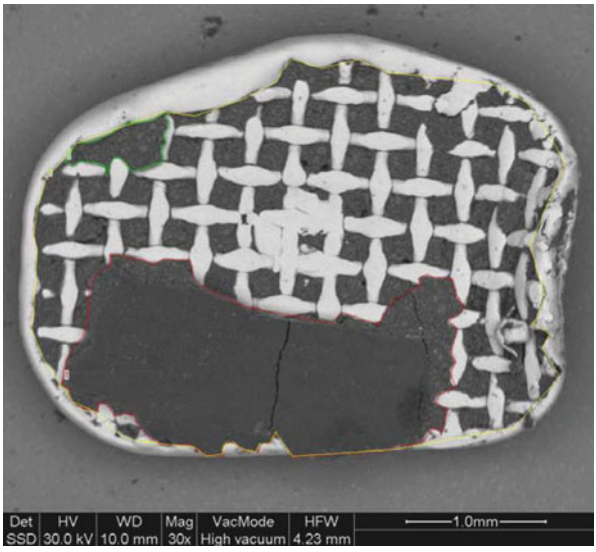

Fig. 1.20 Quantitative evaluation of fracture mode at bracket-resin interface. *Red* and *green lines* outline retained resin, while *yellow line* indicates whole interfacial surface. Areas of three surfaces are quantitatively estimated by image analysis software. Results showed that 34.5 % of total area is covered by retained resin, and thus fracture mode was characterized as 65.5 % adhesive at bracket-resin interface

Micro-CT system mainly consists of an x-ray radiation source, an x-ray detector, and a processing unit which reconstructs the image from the measurements. The latter uses alternatively two reconstruction algorithms commonly known as *iterative method* and *filtered back projection* [95]. The major advantage of this technique is that the bulk analysis is performed nondestructively, allowing the possibility for further analysis at a later time. This is very important when specimens must remain intact through the experimental analysis (e.g., archeological findings and forensics).

The Micro-CT scanning produces hundreds of horizontal slices of the tested sample, as shown in Fig. 1.21. These horizontal slices are used to reconstruct the entire structure, providing information about the geometric features and internal defects of the sample. Additional software can be employed in the development of three-dimensional models, pseudocoloring, and the quantitative analysis of geometrical features of irregular samples (e.g., the total surface area of an orthodontic bracket).

In orthodontics, the quality of soldering between base and wing components of a metallic bracket has been analyzed [96] by a Micro-CT scanner. Large empty spaces were located at the joint interface between the base and wing components (Fig. 1.21).

The clinical efficacy of orthodontic materials and devices is dominated by their mechanical, physical, and electrochemical properties. However, specific properties have distinct clinical implications.

- Modulus of elasticity determines the imposed elastic strain. The higher the modulus, the higher force demanded to achieve the same elastic strain. In alternative expression Ni-Ti alloy deforms the same extent with Co-Cr loaded with lower external forces.
- Clinicians should avoid the great differences in hardness between orthodontic archwires and brackets to minimize the fragment release due to wear between them.
- Fracture toughness is indicative for the resistance of materials to crack propagation. Orthodontic materials (i.e., aesthetics brackets made of various ceramics) are more prone to brittle fracture.
- Electrochemical properties of metallic orthodontic materials must be taken into account especially in order to avoid galvanic phenomena under clinical conditions.
- The majority of the methods described in this chapter can be effectively used to characterize retrieved orthodontic devices in order to describe the underlying aging mechanism providing fundamental information for further research and development of new materials and/or devices.

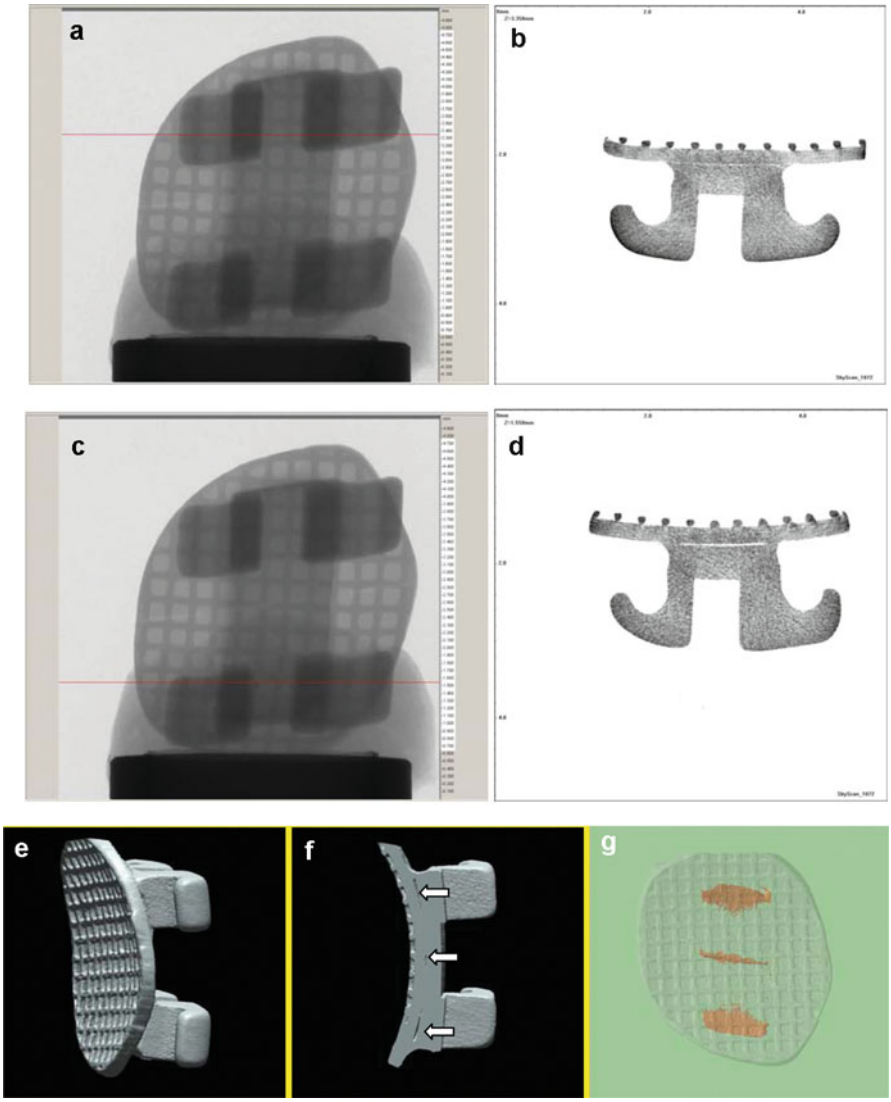

Fig. 1.21 Three-dimensional x-ray microtomographic images and three-dimensional model of metallic orthodontic bracket. (**a**, **c**) X-ray images of specimen. (**b**, **d**) Horizontal cross sections at level of *red line* in images (**a**) and (**c**), respectively. Wing and base components are readily distinguished. Gap between wing and the base is clearly shown in (**d**). (**e**) Three-dimensional model of scanned bracket. (**f**) Details of section of three-dimensional model at base-wing interface, showing presence of gaps (*arrows*). (**g**) Reconstructed image of empty spaces, showing gaps (*orange color*). Base component is also outlined

References

1. Brantley WA, Eliades T (eds) (2001) Orthodontic materials: scientific and clinical aspects. Thieme, Stuttgart, Chapters 2–4, 7 and 8
2. Miura F, Mogi M, Ohura Y, Hamanaka H (1986) The super-elastic property of the Japanese NiTi alloy wire for use in orthodontics. Am J Orthod Dentofacial Orthop 90:1–10
3. Anusavice KJ et al (2003) Mechanical properties of dental materials. In: Phillips' science of dental materials, 11th edn. Saunders/Elsevier Science, St. Louis, Chapter 4
4. Dieter GE (1986) Mechanical metallurgy, 3rd edn. McGraw-Hill, New York, Chapters 8 and 11
5. Asgharnia MK, Brantley WA (1986) Comparison of bending and tension tests for orthodontic wires. Am J Orthod 89:228–236
6. Verstrynge A, Van Humbeeck J, Willems G (2006) In-vitro evaluation of the material characteristics of stainless steel and beta-titanium orthodontic wires. Am J Orthod Dentofacial Orthop 130:460–470
7. Burstone CJ, Goldberg AJ (1983) Maximum forces and deflections from orthodontic appliances. Am J Orthod 84:95–103
8. Burstone CJ, Qin B, Morton JY (1985) Chinese NiTi wire – a new orthodontic alloy. Am J Orthod 87:445–452
9. Andreasen GF, Morrow RE (1978) Laboratory and clinical analyses of nitinol wire. Am J Orthod 73:142–151
10. Khier SE, Brantley WA, Fournelle RA (1991) Bending properties of superelastic and non-superelastic nickel-titanium orthodontic wires. Am J Orthod Dentofacial Orthop 99: 310–318
11. American Dental Association Specification No. 32 for orthodontic wires not containing precious metals (1977) J Am Dent Assoc 95:1169–1171
12. American Dental Association/Council on Scientific Affairs. ANSI/ADA Specification No. 32– Orthodontic Wires (2000)
13. Scott GE Jr (1988) Fracture toughness and surface cracks – the key to understanding ceramic brackets. Angle Orthod 58:5–8
14. Kusy RP (1988) Morphology of polycrystalline alumina brackets and its relationship to fracture toughness and strength. Angle Orthod 58:197–203
15. Kingery WD, Bowen HK, Uhlmann DR (1976) Introduction to ceramics, 2nd edn. Wiley, New York, pp 791–797
16. Taira M, Nomura Y, Wakasa K, Yamaki M, Matsui A (1990) Studies on fracture toughness of dental ceramics. J Oral Rehabil 17:551–563
17. Scherrer SS, Kelly JR, Quinn GD, Xu K (1999) Fracture toughness (KIc) of a dental porcelain determined by fractographic analysis. Dent Mater 15:342–348
18. Fischer H, Marx R (2002) Fracture toughness of dental ceramics: comparison of bending and indentation method. Dent Mater 18:12–19
19. Maehara S, Fujishima A, Hotta Y, Miyazaki T (2005) Fracture toughness measurement of dental ceramics using the indentation fracture method with different formulas. Dent Mater J 24:328–334
20. Wang H, Pallav P, Isgro G, Feilzer AJ (2007) Fracture toughness comparison of three test methods with four dental porcelains. Dent Mater 23:905–910
21. Morena R, Lockwood PE, Fairhurst CW (1986) Fracture toughness of commercial dental porcelains. Dent Mater 2:58–62
22. Smart K, Lancaster D, Sarkar N (1992) Microstructure and fracture toughness of three ceramic brackets. J Dent Res 71(AADR Abstracts):227
23. Pham GN (1999) Fracture characteristics of five polycrystalline alumina orthodontic brackets [MS thesis]. The Ohio State University, Columbus
24. Pham GN, Brantley WA, Mitchell JC, Johnston WM, Webb CS (2000) Fracture characteristics, hardness and grain size of five alumina brackets. J Dent Res 79(IADR Abstracts):548

25. Tilson TF (1994) Evaluation of the fracture toughness of the Japanese Yttrium-stabilized Zirconia orthodontic brackets and possible clinical implications [MS thesis]. The Ohio State University, Columbus
26. Tilson TF, Brantley WA, Johnston WM (1995) Fracture toughness of zirconia ceramic orthodontic brackets. J Dent Res 74(AADR Abstracts):74
27. Fiss MR (2002) Breaking force of ceramic bracket Tie-wings: a comparative study [MS thesis]. The Ohio State University, Columbus
28. Mante FK, Brantley WA, Dhuru VB, Ziebert GJ (1993) Fracture toughness of high alumina core dental ceramics: the effect of water and artificial saliva. Int J Prosthodont 6:546–552
29. Sarkar NK, Redmond W, Schwaninger B, Goldberg AJ (1983) The chloride corrosion behaviour of four orthodontic wires. J Oral Rehabil 10:121–128
30. Edie JW, Andreasen GF, Zaytoun MP (1981) Surface corrosion of nitinol and stainless steel under clinical conditions. Angle Orthod 51:319–324
31. Schwaninger B, Sarkar NK, Foster BE (1982) Effect of long-term immersion corrosion on the flexural properties of nitinol. Am J Orthod 82:45–49
32. Khier SE (1988) Structural characterization, biomechanical properties, and potentiodynamic polarization behavior of Nickel-Titanium orthodontic wire alloys [PhD dissertation]. Marquette University, Milwaukee
33. Khier SE, Brantley WA (1997) In vitro corrosion measurements of Ni-Ti wrought alloys. Saudi Dent J 9:14–16
34. Anusavice KJ, Brantley WA (2003) Physical properties of dental materials. In: Anusavice KJ (ed) Phillips' science of dental materials, 11th edn. Saunders/Elsevier Science, St. Louis, Chapter 3
35. Kim H, Johnson JW (1999) Corrosion of stainless steel, nickel-titanium, coated nickel-titanium, and titanium orthodontic wires. Angle Orthod 69:39–44
36. Huang HH (2005) Surface characterizations and corrosion resistance of nickel-titanium orthodontic archwires in artificial saliva of various degrees of acidity. J Biomed Mater Res A 74:629–639
37. Clarke B, Carroll W, Rochev Y, Hynes M, Bradley D, Plumley D (2006) Influence of Nitinol wire surface treatment on oxide thickness and composition and its subsequent effect on corrosion resistance and nickel ion release. J Biomed Mater Res A 79:61–70
38. Huang HH, Chiu YH, Lee TH, Wu SC, Yang HW, Su KH, Hsu CC (2003) Ion release from NiTi orthodontic wires in artificial saliva with various acidities. Biomaterials 24:3585–3592
39. Yonekura Y, Endo K, Iijima M, Ohno H, Mizoguchi I (2004) In vitro corrosion characteristics of commercially available orthodontic wires. Dent Mater J 23:197–202
40. Oh KT, Kim KN (2005) Ion release and cytotoxicity of stainless steel wires. Eur J Orthod 27:533–540
41. Schiff N, Boinet M, Morgon L, Lissac M, Dalard F, Grosgogeat B (2006) Galvanic corrosion between orthodontic wires and brackets in fluoride mouthwashes. Eur J Orthod 28:298–304
42. Iijima M, Endo K, Yuasa T, Ohno H, Hayashi K, Kakizaki M, Mizoguchi I (2006) Galvanic corrosion behavior of orthodontic archwire alloys coupled to bracket alloys. Angle Orthod 76:705–711
43. Darabara MS, Bourithis LI, Zinelis S, Papadimitriou GD (2007) Metallurgical characterization, galvanic corrosion, and ionic release of orthodontic brackets coupled with Ni-Ti archwires. J Biomed Mater Res B Appl Biomater 81:126–134
44. Siargos B, Bradley TG, Darabara M, Papadimitriou G, Zinelis S (2007) Galvanic corrosion of metal injection molded (MIM) and conventional brackets with nickel-titanium and copper-nickel-titanium archwires. Angle Orthod 77:355–360
45. Rondelli G, Vicentini B (1999) Localized corrosion behaviour in simulated human body fluids of commercial Ni-Ti orthodontic wires. Biomaterials 20:785–792
46. Neumann P, Bourauel C, Jäger A (2002) Corrosion and permanent fracture resistance of coated and conventional orthodontic wires. J Mater Sci Mater Med 13:141–147

47. Es-Souni M, Es-Souni M, Fischer-Brandies H (2002) On the properties of two binary NiTi shape memory alloys. Effects of surface finish on the corrosion behaviour and in vitro biocompatibility. Biomaterials 23:2887–2894
48. Huang HH (2005) Variation in corrosion resistance of nickel-titanium wires from different manufacturers. Angle Orthod 75:661–665
49. Pun DK, Berzins DW (2008) Corrosion behavior of shape memory, superelastic, and nonsuperelastic nickel-titanium-based orthodontic wires at various temperatures. Dent Mater 24:221–227
50. Wang J, Li N, Rao G, Han EH, Ke W (2007) Stress corrosion cracking of NiTi in artificial saliva. Dent Mater 23:133–137
51. Kaneko K, Yokoyama K, Moriyama K, Asaoka K, Sakai J, Nagumo M (2003) Delayed fracture of beta titanium orthodontic wire in fluoride aqueous solutions. Biomaterials 24:2113–2120
52. Ogawa T, Yokoyama K, Asaoka K, Sakai J (2004) Hydrogen absorption behavior of beta titanium alloy in acid fluoride solutions. Biomaterials 25:2419–2425
53. Schiff N, Grosgogeat B, Lissac M, Dalard F (2004) Influence of fluoridated mouthwashes on corrosion resistance of orthodontics wires. Biomaterials 25:4535–4542
54. Yokoyama K, Kaneko K, Ogawa T, Moriyama K, Asaoka K, Sakai J (2005) Hydrogen embrittlement of work-hardened Ni-Ti alloy in fluoride solutions. Biomaterials 26:101–108
55. Walker MP, White RJ, Kula KS (2005) Effect of fluoride prophylactic agents on the mechanical properties of nickel-titanium-based orthodontic wires. Am J Orthod Dentofacial Orthop 127:662–669
56. Cioffi M, Gilliland D, Ceccone G, Chiesa R, Cigada A (2005) Electrochemical release testing of nickel-titanium orthodontic wires in artificial saliva using thin layer activation. Acta Biomater 1:717–724
57. Ahn HS, Kim MJ, Seol HJ, Lee JH, Kim HI, Kwon YH (2006) Effect of pH and temperature on orthodontic NiTi wires immersed in acidic fluoride solution. J Biomed Mater Res B Appl Biomater 79:7–15
58. Kao CT, Ding SJ, He H, Chou MY, Huang TH (2007) Cytotoxicity of orthodontic wire corroded in fluoride solution in vitro. Angle Orthod 77:349–354
59. Li X, Wang J, Han EH, Ke W (2007) Influence of fluoride and chloride on corrosion behavior of NiTi orthodontic wires. Acta Biomater 3:807–815
60. Eliades T, Eliades G, Athanasiou AE, Bradley TG (2000) Surface characterization of retrieved NiTi orthodontic archwires. Eur J Orthod 22:317–326
61. Eliades T, Zinelis S, Papadopoulos MA, Eliades G, Athanasiou AE (2004) Nickel content of as-received and retrieved NiTi and stainless steel archwires: assessing the nickel release hypothesis. Angle Orthod 74:151–154
62. Es-Souni M, Es-Souni M, Fischer-Brandies H (2005) Assessing the biocompatibility of NiTi shape memory alloys used for medical applications. Anal Bioanal Chem 381:557–567
63. Es-Souni M, Fischer-Brandies H, Es-Souni M (2003) On the in vitro biocompatibility of Elgiloy, a Co-based alloy, compared to two titanium alloys. J Orofac Orthop 64:16–26
64. Cullity BD, Stock SR (2001) Elements of x-ray diffraction, 3rd edn. Prentice-Hall, Upper Saddle River
65. Khier SE, Brantley WA, Fournelle RA (1988) Structure and mechanical properties of as-received and heat-treated stainless steel orthodontic wires. Am J Orthod Dentofacial Orthop 93:206–212
66. Brantley W, Webb C, Soto U, Wu Q, Cassinelli A (1998) X-ray diffraction and Vickers hardness of titanium-containing orthodontic wires. J Dent Res 77(AADR Abstracts):108
67. Thayer TA, Bagby MD, Moore RN, DeAngelis RJ (1995) X-ray diffraction of nitinol orthodontic arch wires. Am J Orthod Dentofacial Orthop 107:604–612
68. Mitchell JC, Brantley WA, Tufekci E, Webb CS (2000) X-ray diffraction analyses of cross-sectioned specimens of titanium-containing orthodontic wires. J Dent Res 79(IADR Abstracts):439

69. Iijima M, Ohno H, Kawashima I, Endo K, Mizoguchi I (2002) Mechanical behavior at different temperatures and stresses for superelastic nickel-titanium orthodontic wires having different transformation temperatures. Dent Mater 18:88–93
70. Iijima M, Ohno H, Kawashima I, Endo K, Brantley WA, Mizoguchi I (2002) Micro x-ray diffraction study of superelastic nickel-titanium orthodontic wires at different temperatures and stresses. Biomaterials 23:1769–1774
71. Iijima M, Brantley WA, Kawashima I, Ohno H, Guo W, Yonekura Y, Mizoguchi I (2004) Micro-x-ray diffraction observation of nickel-titanium orthodontic wires in simulated oral environment. Biomaterials 25:171–176
72. Iijima M, Brantley WA, Baba N, Alapati SB, Yuasa T, Ohno H, Mizoguchi I (2007) Micro-XRD study of beta-titanium wires and infrared soldered joints. Dent Mater 23:1051–1056
73. Iijima M, Brantley WA, Yuasa T, Muguruma T, Kawashima I, Mizoguchi I (2008) Joining characteristics of orthodontic wires with laser welding. J Biomed Mater Res B Appl Biomater 84:147–153
74. Lee JH, Park JB, Andreasen GF, Lakes RS (1988) Thermomechanical study of Ni-Ti alloys. J Biomed Mater Res 22:573–588
75. Yoneyama T, Doi H, Hamanaka H, Okamoto Y, Mogi M, Miura F (1992) Super-elasticity and thermal behavior of Ni-Ti alloy orthodontic arch wires. Dent Mater J 11:1–10
76. Bradley TG, Brantley WA, Culbertson BM (1996) Differential scanning calorimetry (DSC) analyses of superelastic and nonsuperelastic nickel-titanium orthodontic wires. Am J Orthod Dentofacial Orthop 109:589–597
77. Barwart O, Rollinger JM, Burger A (1999) An evaluation of the transition temperature range of super-elastic orthodontic NiTi springs using differential scanning calorimetry. Eur J Orthod 21:497–502
78. Fischer-Brandies H, Es-Souni M, Kock N, Raetzke K, Bock O (2003) Transformation behavior, chemical composition, surface topography and bending properties of five selected 0.016″×0.022″ NiTi archwires. J Orofac Orthop 64:88–99
79. Chen R, Zhi YF, Arvystas MG (1992) Advanced Chinese NiTi alloy wire and clinical observations. Angle Orthod 62:59–66
80. Santoro M, Beshers DN (2000) Nickel-titanium alloys: stress-related temperature transitional range. Am J Orthod Dentofacial Orthop 118:685–692
81. Sauerbrunn SR, Crowe BS, Reading M (1993) Modulated differential scanning calorimetry, Polym Mater Sci Eng 68:269–271
82. Reading M, Hahn BK, Crowe BS (1994) Method and apparatus for modulated differential scanning calorimetry. US Patent 5,346,306, 13 Sept1994
83. Brantley WA, Iijima M, Grentzer TH (2003) Temperature-modulated DSC provides new insight about nickel-titanium wire transformations. Am J Orthod Dentofacial Orthop 124:387–394
84. Brantley WA, Guo W, Clark WAT, Iijima M (2008) Microstructural studies of 35°C Copper Ni-Ti orthodontic wire and TEM confirmation of low-temperature martensite transformation. Dent Mater 24:204–210
85. Brantley WA, Iijima M, Grentzer TH (2002) Temperature-modulated DSC study of phase transformations in nickel-titanium orthodontic wires. Thermochimica Acta 392–393:329–337
86. Metallography and microstructures, vol 9, 1st edn (1985). Materials Park: ASM International, pp 23–27, 28–32
87. Samuels LE (1985) Mechanical grinding abrasion and polishing. In: Metallography and microstructures, vol 9, 1st edn. ASM International, Materials Park, pp 33–47
88. Zinelis S, Annousaki O, Makou M, Eliades T (2005) Metallurgical characterization of orthodontic brackets produced by metal injection molding (MIM). Angle Orthod 75:811–818
89. Zinelis S, Annousaki O, Eliades T, Makou M (2003) Characterization of Titanium orthodontic brackets. J Orofac Orthop 64:426–433
90. Eliades T, Zinelis S, Eliades G, Athanasiou T (2003) Characterization of as-received, retrieved and recycled stainless steel brackets. J Orofac Orthop 64:80–87

91. Zinelis S, Eliades T, Pandis N, Eliades G, Bourauel C (2007) Why do NiTi and CuNiTi archwires fracture intraorally? Fractographic analysis and failure mechanism of in vivo-fractured wires. Am J Orthod Dentofacial Orthop 132:84–89
92. Zinelis S, Annousaki O, Eliades T, Makou M (2004) Elemental composition of brazing alloys in metallic orthodontic brackets. Angle Orthod 74:394–399
93. Eliades G, Brantley WA (2001) Instrumental techniques for study of orthodontic materials. In: Brantley WA, Eliades T (eds) Orthodontic materials: scientific and clinical aspects. Thieme, Stuttgart, Chapter 3
94. Schuster S, Eliades G, Zinelis S, Eliades T, Bradley G (2004) Structural conformation and leaching from in vitro-aged and retrieved Invisalign appliances. Am J Orthod Dentofacial Orthop 126:725–728
95. Natali AN, Viola MM (2003) Computer tomography for virtual models in dental imaging. In: Natali AN (ed) Dental biomechanics. Taylor & Francis, London, Chapter 3
96. Gioka C, Bourauel C, Zinelis S, Eliades T, Silikas N, Eliades G (2004) Titanium orthodontic brackets: structure, composition, hardness and ionic release. Dent Mater 20:693–700